The Journal of Chemical Physics

Self-assembly behavior of ABA coil-rod-coil triblock copolymers: A Brownian dynamics simulation approach

Cite as: J. Chem. Phys. **135**, 014102 (2011); https://doi.org/10.1063/1.3606396
Submitted: 20 October 2010 . Accepted: 02 June 2011 . Published Online: 05 July 2011

Yongliang Li, Shaoliang Lin, Xiaohua He, Jiaping Lin, and Tao Jiang

Self-assembly behavior of ABA coil-rod-coil triblock copolymers: A Brownian dynamics simulation approach

Yongliang Li,[1] Shaoliang Lin,[1,a)] Xiaohua He,[2] Jiaping Lin,[1,a)] and Tao Jiang[1]
[1]*Shanghai Key Laboratory of Advanced Polymeric Materials, Key Laboratory for Ultrafine Materials of Ministry of Education, School of Materials Science and Engineering, East China University of Science and Technology, Shanghai 200237, China*
[2]*Department of Chemistry, East China Normal University, Shanghai 200062, China*

(Received 20 October 2010; accepted 2 June 2011; published online 5 July 2011)

The self-assembly behavior of ABA coil-rod-coil triblock copolymers in a selective solvent was studied by a Brownian molecular dynamics simulation method. It was found that the rod midblock plays an important role in the self-assembly of the copolymers. With a decrease in the segregation strength, ε_{RR}, of rod pairs, the aggregate structure first varies from a smecticlike disk shape to a long twisted string micelle and then to small aggregates. The influence of the block length and the asymmetry of the triblock copolymer on the phase behavior were studied and the corresponding phase diagrams were mapped. It was revealed that the variation of these parameters has a profound effect on microstructure. The simulation results are consistent with experimental results. Compared to rod-coil diblock copolymers, the coil-rod-coil triblock copolymers has a larger entropy penalty associated with the interfacial grafting density of the aggregate, leading to a higher ε_{RR} value for structural transitions. © *2011 American Institute of Physics*. [doi:10.1063/1.3606396]

I. INTRODUCTION

The microstructures self-assembled from block copolymers containing rod blocks formed in both solution and the melt have received much attention.[1–11] The nature of chain rigidity impacts the self-assembled supramolecular structures significantly, due to the tendency of rod blocks to form ordered domains. Up to now, most work has focused on the self-assembly behavior of rod-coil diblock copolymers. It is interesting to study the coil-rod-coil triblock copolymers, because more complicated microstructures can be formed compared to the rod-coil diblock copolymers.

Triblock copolymers can form various complex microstructures by self-assembly, including vesicles, spherical micelles, cylindrical micelles, lamellae, hexagonal columnar, bicontinuous cubic, and body-centered tetragonal superlattice in either solution or the melt.[12–14] In contrast to classical coil blocks, the rigidity of the chain blocks results in a special molecular packing due to its liquid crystalline character, causing the copolymers to aggregate into various thermodynamically stable supramolecular structures.[15–21] Li *et al.* synthesized a coil-rod-coil triblock copolymer consisting of oligo (*p*-phenylene-ethynylene) as the rodlike block and polystyrene as the coillike block.[19] It was shown that the segregation of these triblock copolymers in solution could be controlled by manipulating the solvent composition, thus demonstrating a unique solvatochromatic behavior. Huang *et al.* have reported an amphiphilic PEG_{1500}-*b*-EMAP-*b*-PEG_{1500} ABA coil-rod-coil triblock copolymers consisting of poly(ethyleneglycol) (PEG) and an emeraldine aniline-pentamer (EMAP).[20,21] The copolymers were observed to aggregate into a "sandglass" shape in concentrated solutions.

Computer simulation has played an important role in investigating the phase behavior of block copolymers. So far, most simulation work concerns ABA triblock copolymers containing coil blocks.[22–27] Studies of the phase behavior of ABA triblock copolymers having rigid blocks are limited.[28–31] AlSunaidi *et al.* investigated liquid-crystalline ordering in coil-rod-coil triblock copolymers using the dissipative particle dynamics (DPD) method.[28,29] When the systems were cooled down below the order-disorder transition temperature, the isotropic disordered phases turned into a smectic-C phase. Chen *et al.* studied the self-assembly of symmetric coil-rod-coil ABA triblock copolymer melts using self-consistent field lattice techniques in three-dimensional space.[30,31] Various aggregate morphologies, including lamellar, wave lamellar, gyroid, perforated lamellar, cylindrical, and sphericallike phases, were observed when the volume fractions of the rod block were changed. However, all of these investigations focused on the liquid-crystalline behavior or phase-separation behavior of the coil-rod-coil copolymers in melts.

Only a limited amount of work on computer simulation of the self-assembly behavior of copolymers containing rod blocks in solution has been reported in the literature.[32–38] Horsch *et al.* investigated the phase behavior of rod-coil block copolymers based on a coarse-grained model in solution by applying a Brownian dynamics method.[32–34] With increasing concentration, the copolymers self-assemble into spherical micelles with body-centered-cubic (bcc) order, long micelles with nematic order, hexagonal cylinders, tetragonal perforated phases, a hexagonal perforated phase, and a smectic-C lamellar phase. However, so far there has been no work reported on the computer simulation of micellization behavior of coil-rod-coil triblock copolymers in solution.

a)Authors to whom correspondence should be addressed. Electronic addresses: linshaoliang@hotmail.com and jplinlab@online.sh.cn.

In our previous work, we performed a Brownian dynamic simulation on the self-assembly of rod-coil diblock copolymers in solutions.[37] A coarse-grained spring hard bead model was constructed to represent the diblock copolymers. The rigidity of the rod block was realized through an angle bending potential. We found that the rod-coil copolymers in solution can form a novel twisted string in addition to a disk structure. We also extended this work to study the influence of chain conformation on the aggregate structures formed by diblock copolymers as the core-forming block was changed from rigid to flexible.[38]

In the present simulation, we extend the coarse grained model to represent an ABA coil-rod-coil triblock copolymer. The micellization behavior of such copolymers in solution was investigated by the Brownian dynamics method. As far as we know, this is the first example of simulation work on the self-assembly behavior of ABA coil-rod-coil copolymers in solution. The molecular structure of coil-rod-coil triblock copolymers, which have a higher local grafting density between the conjunct points of the rod and coil pairs than diblock copolymers, significantly affects the packing of rods and the aggregate structure. The influence of the segregation strength of rod pairs and block lengths on micellization behavior was studied. In addition, the effect of asymmetry of the coil blocks was also considered. The simulation results are useful for understanding the mechanism for aggregation behavior of coil-rod-coil triblock copolymers.

II. COMPUTATIONAL METHODS

The simulations were performed using a coarse-grained molecular dynamics program (COGNAC) of OCTA. The simulator was developed by Doi's group and is publicly available on their website.[39] COGNAC uses the reduced unit system for setting data. To convert it to real units, a set of unit parameters was used, as described in our previous paper.[37]

A. Model

The triblock copolymer was modeled through a series of beads linked in a linear geometry. The bond potential, U_{bond}, and the angle potential, U_{angle}, of the bonds connecting the beads (atoms) to form a linear chain were given different degrees of rigidity in order to construct the model.

A model combining two A-blocks with n beads and a B-block with m beads, named as $A_nB_mA_n$, was constructed in this work. Figure 1 shows the rendering of the copolymer molecule model $A_6B_6A_6$, in which the beads colored red and green show the rod and coil blocks of the molecule, respectively. A harmonic bonding potential was applied to link these beads, as defined by

$$U_{\text{bond}}(\theta) = \tfrac{1}{2}k_b(r - r_0)^2, \tag{1}$$

where k_b is the bond spring constant and r_0 is the equilibrium bond length. U_{bond} (r) consists of the potentials of the bonds in the A- and B-blocks and the junction bond of between these two blocks. The values of k_b and r_0 are the same as those used in previous work.[37]

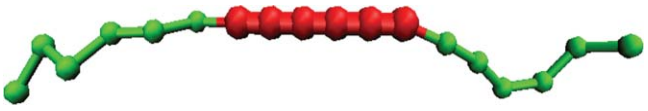

FIG. 1. The layout of $A_6B_6A_6$ coil-rod-coil triblock copolymer. The beads colored red and green are the hydrophobic rod block and the hydrophilic coil block, respectively.

The angle potential was applied to control the angle formed by three linked beads in order to adjust the rigidity of the rod block. For the flexible block, no angle potential was applied. We used a cosine harmonic function to constrain the B-block as

$$U_{\text{angle}}(\theta) = \tfrac{1}{2}k_a(\cos\theta - \cos\theta_0)^2, \tag{2}$$

where k_a is the angle spring constant and θ_0 is the equilibrium angle. The larger the value of k_a, the more rigid is the chain.[40] To obtain a rigid B-block, the values of the equilibrium angle θ_0 and the constant k_a were set to 0.1° and 10 000, respectively.

B. Amphiphilic behavior

A nonbonding potential was used to describe the intermolecular interactions between different beads. To study the self-assembly behavior resulting from solvent selectivity, the following rules for poor and good solvents were applied. If the blocks are hydrophilic, the nonbonding interactions between their beads were described by a purely repulsive interaction potential. If the blocks are hydrophobic, the nonbonding interactions between their beads are modeled with an attractive component. The interaction energy U_{ij} is given by the standard Lennard-Jones (LJ) 12:6 potential acting between any pair of beads i and j:

$$U_{ij} = \begin{cases} 4\varepsilon_{ij}\left[\left(\frac{\sigma_{ij}}{r_{ij}}\right)^{12} - \left(\frac{\sigma_{ij}}{r_{ij}}\right)^{6} - \left(\frac{\sigma^{ij}}{r_{ij}^c}\right)^{12} + \left(\frac{\sigma_{ij}}{r_{ij}^c}\right)^{6}\right], & r \le r_{ij}^c, \\ 0, r > r_{ij}^c \end{cases} \tag{3}$$

where r_{ij}^c is the cutoff distance and $r_{ij} = |\vec{r}_i - \vec{r}_j|$, with $\vec{r}_i$ and $\vec{r}_j$ being the locations of the ith and jth beads, respectively. As in the model employed in our previous work,[37] the interaction between A-A and A-B is repulsive with the cutoff distances, r_{AA}^c and r_{AB}^c, set to a value of $2^{1/6}$. The cutoff, r_{BB}^c, is set to be 2.5, to provide an attractive interaction between B-B blocks. The diameter, σ, of the LJ bead is kept at unity for any pair of species. In this work, the attractive force between the rod blocks is adjusted through the pairwise interaction, ε_{RR}, as a variable, while the other interactions are all set to be unity ($\varepsilon_{RC} = \varepsilon_{CC} = 1.0$). Because there is no explicit solvent particle in a Browian Dynamic simulation, ε_{RR} is related to the solvent selectivity indirectly. When ε_{RR} has a large value, the LJ interaction among the rod particles becomes stronger. This will lead to a packing of rods, analogous to a poorer solvent effect around them (and vice versa).

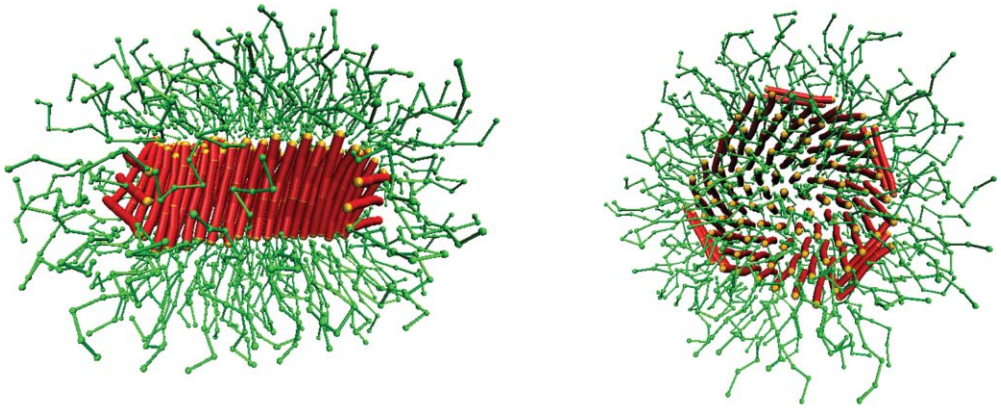

FIG. 2. Snapshot pictures of $A_6B_6A_6$ coil-rod-coil triblock copolymer system with $\varepsilon_{RR} = 3.5$: (a) side view perpendicular to the rod axis; (b) top view along the rod axis.

C. Simulation method

All the simulations were carried out on a cubic cell (60 × 60 × 60) using a Brownian dynamics method developed by Grest and Kremer.[41] The location and velocity of each bead is dominated by the Langevin equation:

$$m_i \frac{d^2\vec{r_i}}{dt^2} = \vec{F_i} - \Gamma \frac{d\vec{r_i}}{dt} + \vec{W}_i(t), \tag{4}$$

where m_i is the mass of the ith bead. $\vec{F_i}$ is the conservative force acting on the ith bead, which is calculated from the potential energies, U_{mol} and U_{ij}, which are related to the location of the ith bead. Γ is the friction constant. In Langevin dynamics, it is assumed that the random force vector is independent of the conservative force because the random forces mimic the effect of solvent particles. There is no temporal correlation in the random force. The amplitude of the random force must satisfy the fluctuation dissipation theorem and therefore meet the following relation:

$$\langle \vec{W}_i(t) \cdot \vec{W}_j(t') \rangle = 6k_B T \Gamma \delta_{ij} \delta(t - t'). \tag{5}$$

A NVT ensemble (i.e., the number of particles, the volume, and the temperature of the system are kept constant) is performed, because the stationary solution of the Langevin equation is the Boltzmann distribution. Periodic boundary conditions were imposed to minimize the effect of finite system size. The initial structure of the system is created through a regular bcc packing lamellar mode and the structure is relaxed by stochastic dynamic simulation. The length of simulation runs was 3×10^6 time steps, i.e., 24 000 time units with an integration time step $\Delta t = 0.008$. All calculations were performed at a temperature $T = 2.0$. To ensure that the self-assembled structure is independent of the box size and the aggregate numbers of the copolymers, we considered systems of $N = 50$, 100, 150, 200, and 250 in a sufficiently large box, where N is the total number of copolymer chains.

III. RESULTS AND DISCUSSION

In the present work, various structures self-assembled from ABA coil-rod-coil triblock copolymers are first studied. The influence of block lengths and the asymmetry of coil blocks on phase behavior and a comparison of the results to experiments, are also made. Finally, a comparison of the self-assembly behavior of triblock copolymers and diblock copolymers is presented.

A. Evolution of micelle structure with changing segregation strength of rod midblocks

Since the aggregation of rod midblocks (B-blocks) is a main driving force in the self-assembly of ABA triblock copolymers, and the segregation strength, ε_{RR}, of rod pairs plays an important role in determining the microstructures, we first present the results of aggregate structure evolution with changing ε_{RR}.

1. Disk micelle

Figure 2 illustrates typical snapshots of the $A_6B_6A_6$ triblock copolymer system with an aggregate number of 100 at a strong segregation strength, $\varepsilon_{RR,}$ of rod pairs. The hydrophilic A-block (coil) is colored green and the hydrophobic B-block (rod) is colored red. In the case of stronger interactions, ε_{RR} = 3.5 (Fig. 2(a)), the aggregated B-blocks tend to align in parallel in the core of the micelle. The packing of the rod blocks results in a kind of lamellar structure. Figure 2(b) shows that the geometric shape of the micelle core is circlelike when viewed from a direction along the B-block alignment axis. Hence, we term this micelle as a "disk (disklike) micelle." Such disk micelle structures can be found at $\varepsilon_{RR} \geq 3.5$.

To describe how the B-blocks within the core of the disk micelle are packed, a typical distance distribution between center positions of the B-blocks at $\varepsilon_{RR} = 3.5$ is plotted in Fig. 3. Several peaks can be seen, with a peak position ratio of 1.11:1.89:2.17:2.95 for the main four peaks. These values are $\sim 1 : \sqrt{3} : 2 : \sqrt{7}$, suggesting that B-blocks are hexagonally packed in the core of the disk micelle.[12]

2. String micelle

At intermediate segregation strengths ($2.5 \leq \varepsilon_{RR} \leq 3.2$), a string (cylinderlike) structure is observed. A typical snapshot for $\varepsilon_{RR} = 3.0$ is shown in Fig. 4. The snapshot

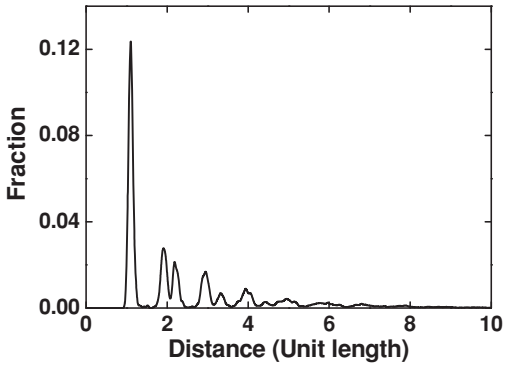

FIG. 3. Distance distribution between center positions of rod blocks for $A_6B_6A_6$ coil-rod-coil triblock copolymers in micelle at $\varepsilon_{RR} = 3.5$. The first four peak position ratio is about $1 : \sqrt{3} : 2 : \sqrt{7}$.

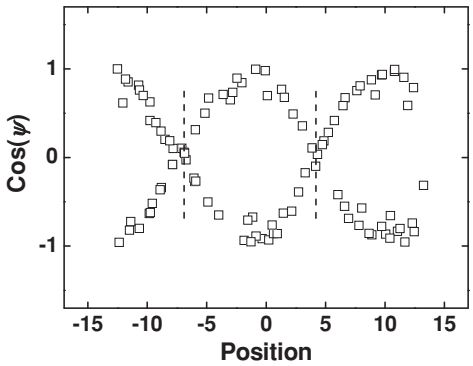

FIG. 5. Vector product $\cos(\psi)$ for the rod alignment as a function of position along the string axis.

shown in Fig. 4(a) illustrates an unusual molecule packing of B-blocks. In each section (plate) of the string micelle, the B-block tends to align along an orientation vector, and this vector gradually rotates along the long-center-axis of the string. That is, the micelle is a twisted string.

The structure of this twisted string exhibits a helical characteristic, where the rod blocks rotate along the long axis of the micelle with the coil blocks forming the covering shell. A mathematical method describing the twisted structure of the rod blocks in the core of a string micelle can be found in Ref. 37. A typical result for the cosine of the twisted angle, $\cos(\psi)$, describing the rod alignment is plotted as a function of position along the axis of the string in Fig. 5. The absolute value of $\cos(\psi)$ gradually decreases to 0, and then increases to 1.0 repeatedly along the string axis. The twisting is almost linear along the axis (at a constant rate of twisting-angular change). This result indicates that the twistable array of rod blocks exists in the core of the string micelle. Here, we can calculate the twisting pitch to be about 10.9 (the distance between dashed lines is shown in Fig. 5).

3. Small aggregates

As the segregation strength, ε_{RR}, decreases, the string micelle breaks into small aggregates, which coexist with some single copolymers (unimers), as can be seen in Fig. 6. We term these broken micelles "small aggregates." With a further decrease in ε_{RR}, more and more unimers come out of the small aggregates. When ε_{RR} is lower than a certain value (critical micelle interaction, CMI), no aggregates remain. And at $\varepsilon_{RR} < 1.7$, only free unimers are found distributed randomly in the system (snapshot not included).

As observed from the snapshots shown in Figs. 2, 4, and 6, the aggregate structure transitions from disk to string and then to small aggregates as the aggregation strength, ε_{RR}, of rod pairs decreases. It can be concluded that the key to understanding these structural transitions is the competition between the enthalpy of the rod blocks, the coil stretching entropy, and the interfacial free energy of the AB blocks. Amphiphilic ABA copolymers can form micelles with B-blocks as the hydrophobic core and A-blocks as the hydrophilic corona. The rigidity of the B-blocks may drive them to align in order to lower the liquid crystalline penalty and minimize the interfacial free energy, while the flexible A-blocks favor random packing to maximize the entropy. The tradeoffs between these effects result in various aggregate structures.

It is reasonable for B-blocks to pack in order to form a disklike structure when the LJ interaction energy, ε_{RR}, of B-beads is high. However, this packing induces a higher density of A-blocks in the micelle corona and at the A-B blocks interface. As ε_{RR} is decreased, the attraction between B-blocks, which tend to align in an ordered fashion, is decreased. Meanwhile, the repulsion of A-blocks starts to dominate, in order to relieve coil stretching. A string micelle is then formed, due to the combination of enthalpic (or energetic) interaction of the B-blocks and the conformational entropy of the A-blocks.

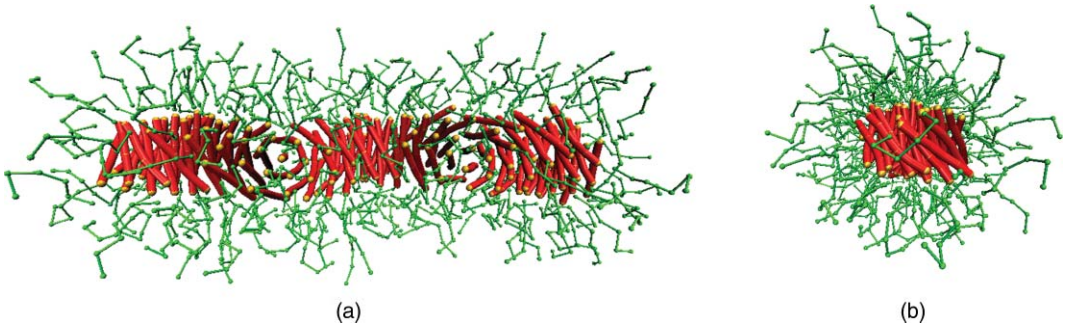

FIG. 4. Snapshot pictures of $A_6B_6A_6$ coil-rod-coil triblock copolymer system with $\varepsilon_{RR} = 3.0$: (a) top view perpendicular to the string axis; (b) side view along the string axis.

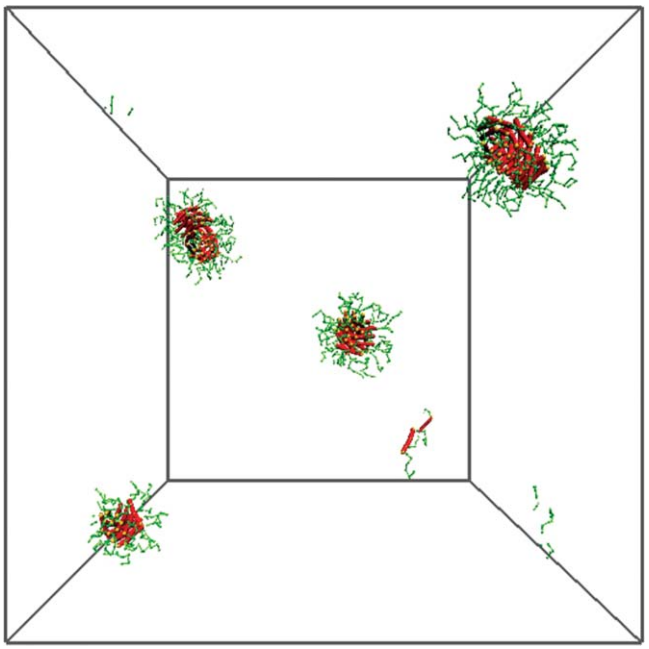

FIG. 6. Snapshot picture of $A_6B_6A_6$ coil-rod-coil triblock copolymer system with $\varepsilon_{RR} = 2.0$.

With a further decrease of ε_{RR}, the attractive interaction of the rod blocks is not strong enough to maintain a long string, while the coil blocks need more space to explore. As a result, the string micelle is broken into small aggregates to ensure that the coil blocks in the shell of the micelles occupy an adequate volume. The small aggregates break further and only unassociated coil-rod-coil triblock copolymers (unimers) exist in the system when the LJ interaction of B-bead pairs is sufficiently low.

To determine if there is an effect due to the box size on the results, we have carried out simulations with systems having 50, 100, 150, 200, and 250 molecules, respectively. It was found that the onset of disklike micelle formation does not change with the number of molecules. However, the plate of the disklike micelle fluctuates more at larger aggregation numbers during the simulation process. The string micelle just becomes longer and more flexible with an increase in the number of molecules. Typical snapshots for the structures of disklike micelles and strings formed by 150 chains are shown in Figs. S1 and S2 (see supplementary material[42]). However, it is worth noticing that the aggregates split into several long micelles when $N = 250$, as shown in Fig. S3 (see supplementary material[42]), suggesting that the long twisted micelle is still a robust phase in large systems.

B. Influence of block lengths and asymmetry of coil blocks on phase diagram

The chain length of copolymers is another important factor determining the stability of micelle structures. The influence of the chain length of the coil-rod-coil triblock copolymers on the micellization behavior will be described in this section. The influence of asymmetry of coil blocks on the phase behavior will also be discussed.

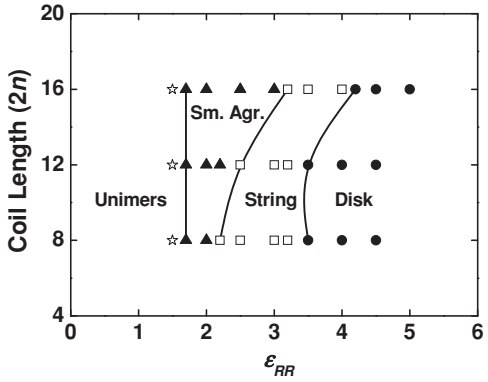

FIG. 7. Phase diagrams for coil-rod-coil triblock copolymers plotted in coil length $2n$ vs. ε_{RR}. Regions of disk (●), string (□), small aggregates (▲), and unimers (☆) are shown.

1. Effects of coil length and rod length

Figure 7 shows a phase diagram where the coil block length $2n$ is plotted against ε_{RR} (with the rod block length fixed at $m = 6$). The phase diagram has regions that are characterized by different microstructures; disks, strings, small aggregates, and unimers. With decreasing ε_{RR} values, microstructures emerge in the sequence: disk micelle to string, to small aggregates, and to unimers. With an increase in the coil length, the onset of disk and string micelle formation both move to higher values of ε_{RR}. Meanwhile, the region characterized by the presence of small aggregates becomes wider and the region consisting of string micelle becomes narrower. From Fig. 7 it can also be seen that at a constant ε_{RR}, the disk micelle is easier to form for shorter coil lengths, while the string structure prefers a longer coil. A less marked effect of the coil length on the CMI is shown in Fig. 7.

Figure 8 shows the influence of rod length of the coil-rod-coil triblock copolymers on micellization behavior. The phase diagram is plotted as rod length m vs. ε_{RR} with a fixed coil bead number $n = 6$. With an increase in the rod length, the onset of disk and string micelle formation moves to lower values of ε_{RR}. Meanwhile, the small aggregates and string micelle phase regions become narrower. From Fig. 8 it is also found that at a constant ε_{RR}, the disk micelle is easy to form for longer rod lengths. Unlike the effect of coil length, a dramatic decrease of the CMI can be observed when the rod length is increased.

Some experimental results describing the micellization behavior of coil-rod-coil triblock copolymers are available in the literature to support our simulation results. Lin *et al.* reported the morphology of aggregates self-assembled from amphiphilic coil-rod-coil triblock copolymers containing conjugated poly[2,7-(9,9-dihexylfluorene)] and coillike poly(2-vinylpyridine) in selective solvents of methanol/tetrahydrofuran.[14] The experimental results show that such copolymers can aggregate into elongated cylinders due to their symmetric structure. Such a cylindrical structure is consistent with our simulation results, where an elongated string micelle can be formed by coil-rod-coil triblock copolymers. Huang *et al.* has studied a coil-rod-coil triblock copolymer of poly(ethylene glycol) (PEG) and an aniline pentamer

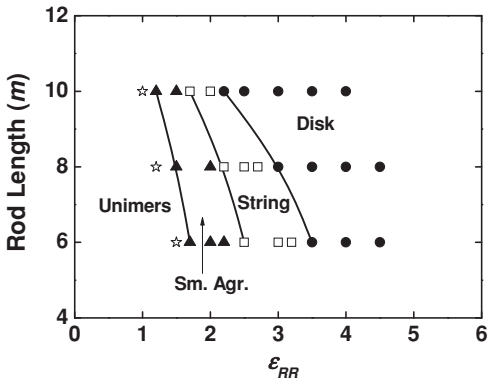

FIG. 8. Phase diagrams for coil-rod-coil triblock copolymers plotted in rod length m vs. ε_{RR}. Regions of disk (●), string (□), small aggregates (▲), and unimers (☆) are shown.

(AP), a PEG-*block*-AP-*block*-PEG system.[21] They found that when the triblock copolymer was added directly into an aqueous solution, it self-assembled spontaneously into spherical aggregates, with an AP rod core and a shell of PEG coil, which is similar to the small aggregates in our simulation prediction.

de Cuendias *et al.* studied the self-assembly behavior of amphiphilic coil-rod-coil copolymer with a central π-conjugated sequence linked to two flexible poly(ethyleneoxide) blocks in water.[13] It was found that the coil-rod-coil triblock copolymers can form small spherical micelles when the rod block is short. Long wormlike micelle structures appear with increasing rod length. This result is in agreement with our simulation predictions. As can be seen in Fig. 8, the triblock copolymers assemble into small aggregates at certain values of ε_{RR}. With increasing rod block length, a string micelle is obtained.

A very interesting finding in the work reported here is that the disklike structure can transform into a long twisted micelle as ε_{RR} is decreased. The transition process from disk to twisted micelle is analogous to a cylindrical phase formed from a hexatic phase in the experimental bulk system.[43] It is also like a helical ribbon observed in many experiments.[44] Selinger *et al.* have done large amounts of theoretical and simulation surveys in order to explain the formation of tubules and helical ribbons in systems of chiral amphiphilic molecules.[45–47] Their theories are based on a continuum elastic free energy that allows a direction of molecular tilt in the curvature of the membrane, showing that the formation of tubules and helical ribbons is driven by the curvature of the membranes, and their predictions are consistent with experiments.[48,49]

Selinger *et al.* further developed an accelerated approach for studying the formation of a chiral helical and twisted ribbon phase through Monte Carlo simulations.[50] A transition from a twisted ribbon with Gaussian saddlelike curvature to a helical ribbon with cylindrical curvature was found as a function of the interaction parameters. The pitch and diameter of the aggregate also changed greatly during the process. An analogous result was also observed by Glotzer's group later. They predict that the flat bilayer sheets of P_2 symmetry assembled by laterally tethered rodlike nanoparticles and their molecular analogues scroll into distinct helical structures.[51] In terms of experiments, Stupp *et al.* reported a torsional strain mechanism that tunes the pitch of micrometer-long helical assemblies.[52] It is found that a bulkier substituent at the terminus of the alkyl segment could be generating torsional strains that drive the formation of the superhelix from the initially cylindrical assemblies. Furthermore, the pitch of the helices appears to depend on the shape and packing of the end groups within the assemblies. Although the coil-rod-coil copolymer model constructed in this article is not a chiral structure, we also found that varying the rod and coil length could greatly affect the width and pitch of the long twisted micelle. So we consider helical architectures ideally suited for the design of responsive materials, since the dynamic and reversible conformational changes can be triggered by a series of external environmental conditions or by modifying the polymer structure through chemical changes.

We tried to find an intermediated state between the disk and long twisted micelle phases during the simulation process through varying the aggregate number and slowly decreasing ε_{RR}. But the results show that there is no stable intermediate state, because the phase transition occurs in a very short time. Unlike the ribbon model employed by Selinger *et al.*, there is no elastic spring among the rod blocks in the simulation process and the rods are non-chiral blocks. So the rods tend to pack at a rather large angle with respect to their neighbours to lower the free energy as the structural transition from disk to string occurs. We consider this to be the main reason for the sudden phase transition.

The twisting pitch of the rod blocks in the core of the string micelle containing various lengths of coil blocks and rod blocks are illustrated in parts (a) and (b) of Fig. 9, respectively. With decreasing segregation strength, ε_{RR}, the pitch decreases. This suggests that the rod blocks are easy to twist at lower values of ε_{RR}. Concomitantly, at a fixed ε_{RR}, a lower value of the pitch can be obtained with an increasing length of coil blocks, as shown in Fig. 9(a). This indicates that longer chain coils make it easier to form a twisted structure in the core of the string micelle. As shown in Fig. 9(b), at a fixed ε_{RR}, the pitch became smaller as the rod length decreases. This confirms that shorter rods prefer to twist within the core.

The dependence of the width of the string on chain length was also studied. It was found that the width increased with an increase in the rod length or the coil length. However, once the string is formed, the width does not change with changing ε_{RR} for a fixed length of triblock copolymers. Meanwhile, the width (diameter) of the core of the string correlates directly with the length of the rod block, but it is uncorrelated with the coil block length. This indicates that the limiting width of the long micelle is determined by the spontaneous twist of the rod block.

On the other hand, we also checked the chirality of the twisted string. It is found that the occurrence of a left or right handed twisted structure is random as the structure transitions from a disk to a string. There is hardly any stationary handedness within the string. The coil-rod-coil copolymers are packed homogeneously in the initial lamellar structure, which has no effect on the twisting behavior of rod blocks. Meanwhile, the rod-coil-rod copolymer model is achiral. So

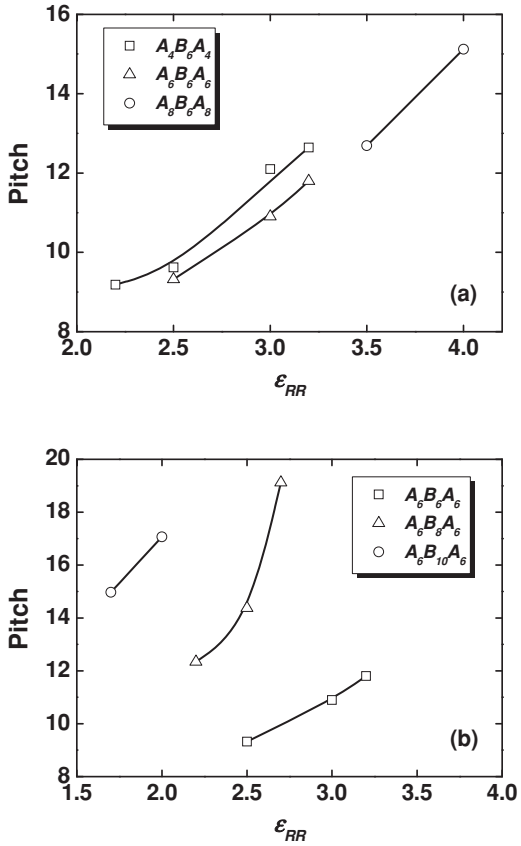

FIG. 9. Dependencies of pitch for the twisting of rod blocks in the core of string structure on the ABA triblock copolymer chain length: (a) coil length; (b) rod length.

the twisted long string forms with either handedness during the twisting process.

2. Effect of asymmetry of triblock copolymer

All of the above simulations were carried out for symmetric coil blocks in ABA triblock copolymers. However, it has been demonstrated that the asymmetry of the outer blocks in ABA-type block copolymers can have a pronounced influence on microphase behaviors.[53–57] In this section, we restrict our attention to the influence of the asymmetry of coil blocks on phase behavior. The asymmetric $A_{n1}B_mA_{n2}$ coil-rod-coil triblock copolymers studied here has 18 beads, where the number m of B-beads is 6, and the total A-beads number of n_1 and n_2 is 12 ($n_1 \geq n_2$). The layout of various $A_{n1}B_6A_{n2}$ coil-rod-coil triblock copolymers are is presented in Fig. 10. The decrease in n_2 (simultaneously increasing n_1) corresponds to an increase in the asymmetry of coil blocks in the triblock copolymer.

Figure 11 shows the influence of asymmetry of coil blocks on the self-assembly behavior. The phase diagram is plotted as the number of beads n_2 in the short coil vs. ε_{RR}. As can be seen, for the asymmetric coil-rod-coil triblock copolymers, the transitions of the aggregate structures from disk, to string, to small aggregates is in the same order as the symmetric copolymers with decreasing ε_{RR}. With increasing n_2, the region of small aggregates becomes wider and the onset of

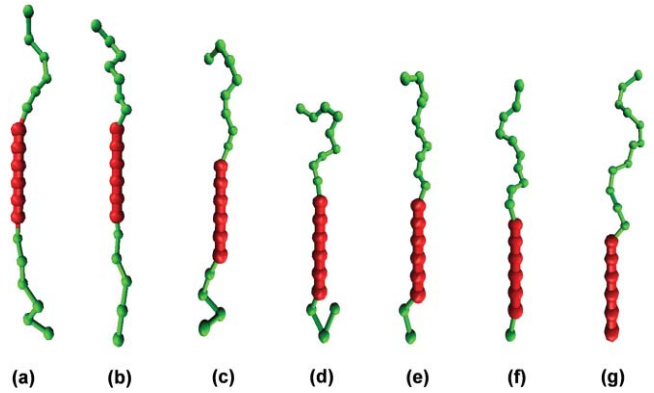

FIG. 10. The layouts of various $A_{n1}B_6A_{n2}$ coil-rod-coil triblock copolymers with a total beads number of 18. (a) $A_6B_6A_6$, (b) $A_7B_6A_5$, (c) $A_8B_6A_4$, (d) $A_9B_6A_3$, (e) $A_{10}B_6A_2$, (f) $A_{11}B_6A_1$, (g) $A_{12}B_6$.

string micelle formation moves to higher ε_{RR}. An interesting feature should be noted that the onset of disk formation does not show a monotonic change. It first increases to a higher ε_{RR} value and then decreases with an increasing asymmetry of coil blocks. The result indicates that the asymmetric coil-rod-coil copolymers prefer to form the long string micelle phase as compared to the symmetric triblock copolymers or (and) the pure diblock copolymers. Meanwhile, a less marked effect on CMI with the change of asymmetry can be observed.

The influence of asymmetry of the coil block on the twisting of rod blocks in the core of the string micelle was also examined. The twisting pitch for various coil block lengths is illustrated in Fig. 12. The twisting pitch of the rod blocks vs. the bead number n_2 of the short coil is plotted at a fixed ε_{RR} value of 3.0. As can be seen from Fig. 12, with decreasing n_2 (increasing the asymmetry of coil blocks), the pitch first decreases and then increases to a high value. It should be noted that the formation of the string structure depends on the combination of enthalpic interactions of the rod blocks and the conformational entropy of the coil blocks. The entropy of the coil blocks is changed by the variation of the asymmetry of the coil blocks, which further results in changing the pitch of the twisting of the rod blocks within the string structures.

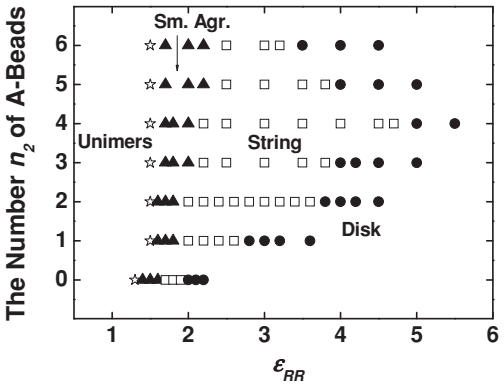

FIG. 11. Simulation phase diagrams for asymmetric $A_{n1}B_6A_{n2}$ coil-rod-coil triblock copolymers plotted in the number n_2 of A-beads of short coil vs. ε_{RR}. Regions of disk (●), string (□), small aggregates (▲), and unimers (☆) are shown.

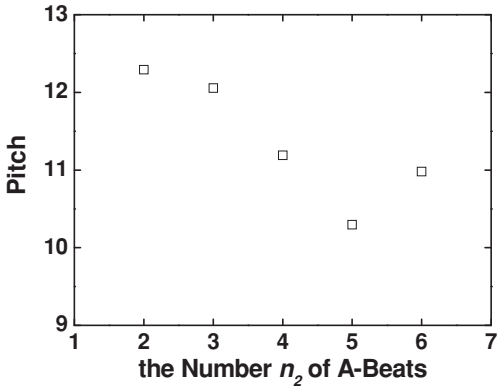

FIG. 12. Dependency of pitch for the twisting of rod blocks in the core of string structure on the asymmetric $A_{n1}B_6A_{n2}$ coil-rod-coil triblock copolymers at $\varepsilon_{RR} = 3.0$.

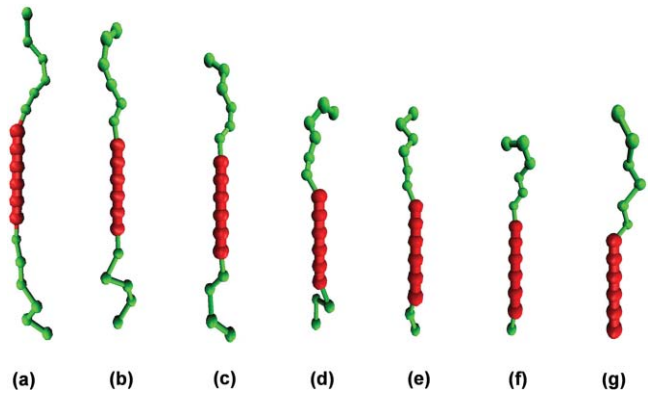

FIG. 13. The layouts of $A_6B_6A_n$ coil-rod-coil triblock copolymers with various A-beads number of short coil. (a) $A_6B_6A_6$, (b) $A_6B_6A_5$, (c) $A_6B_6A_4$, (d) $A_6B_6A_3$, (e) $A_6B_6A_2$, (f) $A_6B_6A_1$, (g) A_6B_6.

We also carried out simulations regarding the influence of asymmetry by changing one coil block length and fixing the other coil block and rod block length. The typical asymmetric coil-rod-coil triblock copolymers, coded as $A_6B_6A_n$, has one rod block with 6 B-beads, one coil block with 6 A-beads, and another coil block with various A-bead number n from 0 to 6. The layout of various $A_6B_6A_n$ coil-rod-coil triblock copolymers is presented in Fig. 13. The effect of changing the bead number of one coil block on the self-assembly behavior of triblock copolymers is illustrated in Fig. 14. A transition sequence of disk to string micelle to small aggregates and unimer phases can be observed as ε_{RR} decreases. With increasing n, corresponding to a decrease in the asymmetry of the coil blocks, the region of small aggregates becomes wider and the onset of string micelle formation moves to higher ε_{RR}. Concomitantly, the onset of disk formation first increases to a higher value of ε_{RR} and then decreases. A less marked effect on CMI was observed. This phase behavior, resulting from an asymmetry generated by varying the length of one coil block, is similar to that illustrated in Fig. 11. However, it should be noted that the self-assembly behavior of $A_6B_6A_n$ illustrated in Fig. 14 combines not only the influence of the asymmetry of the coil blocks, but also the effect of coil chain length. As already presented in Fig. 7, disk formation moves to lower ε_{RR} with decreasing coil length. So the lack of monotonic change in disk formation shown in Fig. 14 also confirms that asymmetry has a profound effect on the self-assembly behavior of triblock copolymers.

C. Comparison of ABA coil-rod-coil triblock copolymer system with AB coil-rod diblock copolymer system

For the asymmetric ABA triblock copolymer, when $n_2 = 0$, it becomes the well-studied AB coil-rod copolymer. It is meaningful to make a comparison between the self-assembly behavior of AB diblock copolymers and ABA triblock copolymers. Figure 15 shows the phase diagram for rod-coil diblock copolymers plotted in as coil length vs. ε_{RR}. The rod-bead number is fixed at 6 and the coil-bead number varies from 8 to 16. In order to compare these two systems it should be noted that the numbers of rod beads and coil beads of the diblock copolymer used here are the same as those of coil-rod-coil triblock copolymers shown in Fig. 7. It is shown in Fig. 15 that the aggregate structure varies from disk micelle, to string micelle, and further to small aggregates and unimers with decreasing ε_{RR} value. With increasing coil length, the onsets for the disk and string micelle formation move to higher values of ε_{RR}. Meanwhile, the region of small aggregates becomes wider and a less marked effect of coil length on the CMI is observed. The rod-coil diblock copolymers shows the same behavior as coil-rod-coil triblock copolymers with increasing coil length, as illustrated in Fig. 7. We also examined the influence of rod length for the diblock copolymer system. A similar self-assembly behavior was observed as compared to the triblock copolymer system. The results indicate that the essence of the self-assembly behavior of these two type copolymers is the same.

Comparing Fig. 7 and Fig. 15, it can be seen that an obvious difference between rod-coil and coil-rod-coil copolymers system is the large disparity for the critical ε_{RR} values of phase transitions. Both the CMI and the onsets of disk and string formation for the coil-rod-coil triblock copolymers have moved to a much higher ε_{RR} value than those of the rod-coil diblock copolymers system. It may be due to the fact

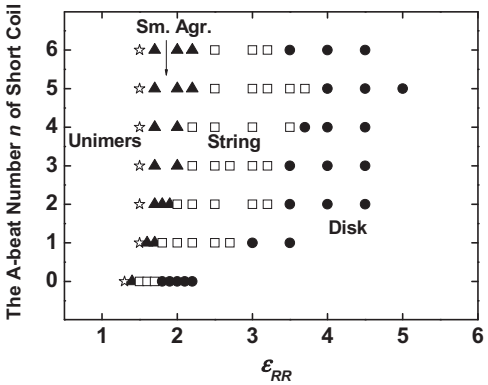

FIG. 14. Simulation phase diagrams for asymmetric $A_6B_6A_n$ coil-rod-coil triblock copolymers plotted in the number n of A-beads of short coil vs. ε_{RR}. Regions of disk (●), string (□), small aggregates (▲), and unimers (☆) are shown.

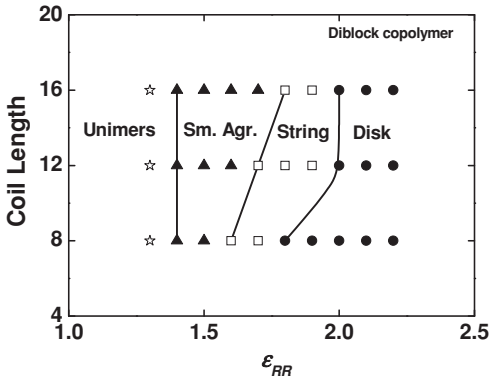

FIG. 15. Phase diagrams for rod-coil diblock copolymers plotted in coil length vs. ε_{RR}. Regions of disk (●), string (□), small aggregates (▲), and unimers (☆) are shown.

that the graft point density of the coil blocks for the triblock copolymers on the surface of the micelle is much higher than that of the diblock copolymers.[58] Compared with rod-coil diblock copolymers, the coil-rod-coil triblock copolymers has two graft points in each molecule as they aggregate. So the coil blocks could not pack alternately on the surface of the rod blocks to lower the local grafting density. During the aggregation process, the density of coil blocks at the interface of the rod and coil blocks becomes much higher. To keep the micelle structure stable, the attraction interaction among the rod pairs should be correspondingly larger to compensate for the increase in the local density penalty of the rod-coil junctions, which leads to a higher ε_{RR} value.

IV. CONCLUSION

A Brownian dynamics method was applied to study the self-assembly of coil-rod-coil triblock copolymers in a selective solvent. The rod blocks tend to pack orientationally in the core to form a disklike micelle, when the segregation strength ε_{RR} of rod blocks is high. With decreasing segregation strength, the rod blocks pack in a twisted manner, leading to a structural transition from disk to string. The string micelle is broken into small aggregates and to unimers with a further decrease of ε_{RR}. The phase diagrams of ABA triblock copolymers show that the CMI and the onset of disk and string formation moves to a higher ε_{RR} value with decreasing the rod length or increasing the coil length. Some simulation results coincide with existing experimental results. The influence of asymmetry of coil blocks on the phase diagram is also presented. With increasing asymmetry of coil blocks, the onset of string moves to lower values of ε_{RR}, while the disk structure tends to form at higher values of ε_{RR}. In contrast to the rod-coil diblock copolymers, the coil-rod-coil triblock copolymers suffer a large entropy penalty of interfacial grafting density of the micelle, leading to a higher ε_{RR} value for structural transitions.

ACKNOWLEDGMENTS

This work was supported by the National Natural Science Foundation of China (50925308) and by the Natural Science Foundation of Shanghai (10ZR1407800). Support from Projects of Shanghai Municipality (11QA1401600, 2007CG38, 09XD1401400, and 0952nm05100) and Fundamental Research Funds for the Central Universities (20100074120001 and WD0914031) is also appreciated.

[1] S. A. Jenekhe and X. L. Chen, Science **283**, 372 (1999).
[2] J. T. Chen, E. L. Thomas, C. K. Ober, and G. P. Mao, Science **273**, 343 (1996).
[3] S. I. Stupp, V. LeBonheur, K. Walker, L. S. Li, K. E. Huggins, M. Keser, and A. Amstutz, Science **276**, 384 (1997).
[4] J. M. L. J. Cornelissen, M. Fischer, N. M. J. A. Sommerdijk, and R. M. J. Nolte, Science **280**, 1427 (1998).
[5] F. Checot, S. Lecommandoux, Y. Gnanou, and H. A. Klok, Angew. Chem., Int. Ed. **41**, 1339 (2002).
[6] A. N. Semenov, Mol. Cryst. Liq. Cryst. **209**, 191 (1991).
[7] D. R. M. Williams and G. H. Fredrickson, Macromolecules **25**, 3561 (1992).
[8] M. Muller and M. Schick, Macromolecules **29**, 8900 (1996).
[9] M. W. Matsen and C. Barrett, J. Chem. Phys. **109**, 4108 (1998).
[10] J. Lin, S. Lin, L. Zhang, and T. Nose, J. Chem. Phys. **130**, 094907 (2009).
[11] L. Liu, J. K. Kim, and M. Lee, ChemPhysChem **9**, 1585 (2008).
[12] M. Lee, D. W. Lee, and B. K. Cho, J. Am. Chem. Soc. **120**, 13258 (1998).
[13] A. de Cuendias, E. Igarboure, S. Lecommandoux, E. Cloutet, and H. Cramail, J. Polym. Sci., Part A: Polym. Chem. **46**, 4602 (2008).
[14] C. H. Lin, Y. C. Tung, J. Ruokolainen, R. Mezzenga, and W. C. Chen, Macromolecules **41**, 8759 (2008).
[15] L. Bu, Y. Qu, D. Yan, Y. Geng, and F. Wang, Macromolecules **42**, 1580 (2009).
[16] M. Knaapila, M. V. Garamus, L. Almasy, J. S. Pang, M. Forster, A. Gutacker, U. Scherf, and A. P. Monkman. J. Phys. Chem. B **112**, 16415 (2008).
[17] L. Rubatat, X. Kong, S. A. Jenekhe, J. Ruokolainen, M. Hojeij, and R. Mezzenga, Macromolecules **41**, 1846 (2008).
[18] J. E. Yang, S. Samal, T. Higashihara, K. Sugiyama, N. Haraguchi, A. Matsuo, A. Hirao, and J. S. Lee, Macromolecules **39**, 3038 (2006).
[19] K. Li, L. Guo, Z. Liang, P. Thiyagarajan, and Q. Wang, J. Polym. Sci., Part A: Polym. Chem. **43**, 6007 (2005).
[20] L. Huang, J. Hu, L. Lang, X. Chen, Y. Wei, and X. Jing, Macromol. Rapid Commun. **28**, 1559 (2007).
[21] L. Huang, J. Hu, L. Lang, X. Zhuang, X. Chen, Y. Wei, and X. Jing, Macromol. Rapid Commun. **29**, 1242 (2008).
[22] X. Li, Y. Liu, L. Wang, M. Deng, and H. Liang, Phys. Chem. Chem. Phys. **11**, 4051 (2009).
[23] X. Li, I. V. Pivkin, H. Liang, and G. E. Karniadakis, Macromolecules **42**, 3195 (2009).
[24] R. Wang, P. Tang, F. Qiu, and Y. L. Yang, J. Phys. Chem. **109**, 17120 (2005).
[25] C. Chaibundit, W. Mingvanish, S. C. Turner, S. M. Mai, J. Patrick, A. Fairclough, A. J. Ryan, M. W. Matsen, and C. Booth, Macromol. Rapid Commun. **21**, 964 (2000).
[26] S. H. Kim and W. H. Jo, Macromolecules **34**, 7210 (2001).
[27] T. Aoyagi, T. Honda, and M. Doi, J. Chem. Phys. **117**, 8153 (2002).
[28] A. AlSunaidi, W. K. den Otter, and J. H. R. Clarke, Philos. Trans. R. Soc. London, Ser. A **362**, 1773 (2004).
[29] A. AlSunaidi, W. K. den Otter, and J. H. R. Clarke, J. Chem. Phys. **130**, 124910 (2009).
[30] J. Z. Chen, C. X. Zhang, Z. Y. Sun, L. J. An, and Z. Tong, J. Chem. Phys. **127**, 024105 (2007).
[31] J. Song, T. Shi, Y. Li, J. Chen, and L. J. An, J. Chem. Phys. **129**, 054906 (2008).
[32] M. A. Horsch, Z. L. Zhang, and S. C. Glotzer, Phys. Rev. Lett. **95**, 056105 (2005).
[33] M. A. Horsch, Z. L. Zhang, and S. C. Glotzer, J. Chem. Phys. **125**, 184903 (2006).
[34] M. A. Horsch, Z. L. Zhang, and S. C. Glotzer, Soft Matter **6**, 945 (2010).
[35] N. Yoshinaga and K. Yoshikawa, J. Chem. Phys. **127**, 044902 (2007).
[36] L. He, L. Zhang, Y. Ye, and H. Liang, J. Phys. Chem. B **114**, 7189 (2010).
[37] S. Lin, N. Numasawa, T. Nose, and J. Lin, Macromolecules **40**, 1684 (2007).
[38] S. Lin, X. He, Y. Li, J. Lin, and T. Nose, J. Phys. Chem. B **113**, 13926 (2009).
[39] See http://octa.jp for the description of OCTA software.

[40]S. Lin, N. Numasawa, T. Nose, and J. Lin, Mol. Cryst. Liq. Cryst. **466**, 53 (2007).
[41]G. S. Grest and K. Kremer, Phys. Rev. A **33**, 3628 (1986).
[42]See supplementary material at http://dx.doi.org/10.1063/1.3606396 for aggregate structures formed by $A_6B_6A_6$ coil-rod-coil triblock copolymer system with various chain numbers.
[43]M. Lee, B. Cho, Y. Jang, and W. Zin, J. Am. Chem. Soc. **122**, 7449 (2000).
[44]C. Sung, L. Kung, C. Hsu, T. Lin, and R. Ho, Chem. Mater. **18**, 352 (2006).
[45]J. V. Selinger, M. S. Spector, and J. M. Schnur, J. Phys. Chem. B **105**, 7158 (2001).
[46]J. V. Selinger, F. C. MacKintosh, and J. M. Schnur, Phys. Rev. E **53**, 3804 (1996).
[47]J. V. Selinger and J. M. Schnur, Phys. Rev. Lett. **71**, 4091 (1993).
[48]Y. M. Lvov, R. R. Price, J. V. Selinger, A. Singh, M. S. Spector, and J. M. Schnur, Langmuir **16**, 5932 (2000).
[49]M. S. Spector, J. V. Selinger, A. Singh, J. M. Rodriguez, R. R. Price, and J. M. Schnur, Langmuir **14**, 3493 (1998).
[50]R. L. B. Selinger, J. V. Selinger, A. P. Malanoski, and J. M. Schnur, Phys. Rev. Lett. **93**, 158103 (2004).
[51]T. D. Nguyen and S. C. Glotzer, Small **5**, 2092 (2009).
[52]L. Li, H. Jiang, B. W. Messmore, S. R. Bull, and S. I. Stupp, Angew. Chem., Int. Ed. **46**, 5873 (2007).
[53]I. C. Riegel, F. M. de Bittencourt, O. Terrau, A. Eisenberg, C. L. Petzhold, and D. Samios, Pure Appl. Chem. **76**, 123 (2004).
[54]R. Adhikari, T. A. Huy, M. Buschnakowski, G. H. Michler, and K. Knoll, New J. Phys. **6**, 28 (2004).
[55]M. W. Maten, J. Chem. Phys. **113**, 5539 (2000).
[56]S. D. Smith, M. W. Hamersky, M. K. Bowman, K. Ø. Rasmussen, and R. J. Spontak, Langmuir **22**, 6465 (2006).
[57]A. Soldera, Y. Qi, and W. T. Capehart, J. Chem. Phys. **130**, 064902 (2009).
[58]A. Halperin, Macromolecules **23**, 2724 (1990).